Ruthenium-Cathepsin Inhibitor Conjugates for Green Light-Activated Photodynamic Therapy and Photochemotherapy

Madeline Denison,¹ Santana P. Garcia,² Alexander Ullrich,³ Izabela Podgorski,^{4,5} Heather Gibson,^{3,5} Claudia Turro,^{2*} and Jeremy J. Kodanko^{1,5*}

Abstract. Dysregulated cathepsin activity is linked to various human diseases, including metabolic disorders, autoimmune conditions, and cancer. Given the overexpression of cathepsin in the tumor microenvironment, cathepsin inhibitors are promising pharmacological agents and drug delivery vehicles for cancer treatment. In this study, we describe the synthesis, photochemical and biological assessment of a dual-action agent based on ruthenium that is conjugated with a cathepsin inhibitor, designed for both photodynamic therapy (PDT) and photochemotherapy (PCT). The ruthenium-cathepsin inhibitor conjugate was synthesized through an oxime click reaction, combining a pan-cathepsin inhibitor based on E64d with the Ru(II) PCT/PDT fragment [Ru(dqpy)(dppn)], where dqpy = 2,6-di(quinoline-2-yl)pyridine and dppn = benzo[i]-dipyrido[3,2a:2',3'-c|phenazine. Photochemical investigations validated the conjugate's ability to release a triazole-containing cathepsin inhibitor for PCT and to generate singlet oxygen for PDT upon exposure to green light. Inhibition studies demonstrated the conjugate's potent and irreversible inactivation of purified and intracellular cysteine cathepsins. Two Ru(II) PCT/PDT agents based on the [Ru(dqpy)(dppn)] moiety were evaluated for photoinduced cytotoxicity in 4T1 murine triple-negative breast cancer cells, L929 fibroblasts, and M0, M1, and M2 macrophages. The cathepsin inhibitor conjugate displayed notable selectivity for inducing cell death under irradiation compared to dark conditions, mitigating toxicity in the dark observed with the triazole control

¹Department of Chemistry, Wayne State University, 5101 Cass Ave, Detroit, MI 48202

²Department of Chemistry and Biochemistry, The Ohio State University, Columbus, Ohio 43210

³Department of Oncology, Wayne State University, Detroit, MI 48201

⁴Department of Pharmacology, School of Medicine, Wayne State University, Detroit, MI 48201

⁵Karmanos Cancer Institute, Detroit, Michigan 48201

complex $[Ru(dqpy)(dppn)(MeTz)]^{2+}$ (MeTz = 1-methyl-1*H*-1,2,4-triazole). Notably, our lead complex is among a limited number of dual PCT/PDT agents activated with green light.

Introduction

Cancer is the second leading cause of death worldwide, attributing to nearly 10 million global deaths in 2020.¹ While recent advancements in screening technology and treatment have resulted in a steady decline in the cancer death rate by 1.5% from 2019 to 2020,² it is evident preventative measures and new treatments must continue to progress. While traditional chemotherapy is effective in killing rapidly differentiating cells, it generally cannot discern between cancerous and normal cells, resulting in unwanted side effects. To combat this problem, light activated therapy, such as photodynamic therapy (PDT), has evolved to trigger medicinal effects solely in irradiated areas. In traditional PDT agents, excitation of photosensitizer with visible light results in the formation of the long-lived $^3\pi\pi^*$ state, where upon relaxation back to the singlet ground state (1 GS), energy is transferred to ground-state triplet oxygen (3 O₂) to form singlet oxygen (1 O₂), a type of reactive oxygen species (ROS). Light activation enables spatiotemporal control of ROS generation to induce oxidative damage in an area of interest, such as tumors, while avoiding toxicity in normal tissue.

PDT agents have evolved since Photofrin was first clinically approved in 1993, and Ru(II)-based complexes have been explored as potential photoactivated therapeutics. The rich photophysical properties,³ ability to intercalate between DNA bases through π -extended ligands,⁴⁻⁶ and improved water solubility and resistance to photobleaching over porphyrins make Ru(II) complexes attractive PDT candidates.⁷⁻¹³ Unfortunately, a large disadvantage of potential Ru(II) PDT agents is that their photochemistry is generally restricted to blue light activation, limiting the

treatment to superficial tissues. Thus, ligands with larger π -systems have been investigated coordinated to Ru(II) centers with the goals of increasing absorptivity in the visible range, lower the energy of ${}^3\pi\pi^*$ state to increase the excited state lifetimes, and to red-shift the absorption towards the "PDT window" (from 600–1100 nm). Specifically, Ru(II) photosensitizer TLD-1433 contains an imidazo[4,5-f][1,10]phenanthroline (IP) ligand conjugated to an α -terthienyl group for improved electron delocalization and absorptivity, allowing for green-light activation. As a consequence, TLD-1433 has advanced to Phase II clinical trials to treat non-muscle-invasive bladder cancer, demonstrating the clinical relevance of Ru(II)-based PDT.

An additional light activated approach for cancer treatment is photochemotherapy (PCT). PCT utilizes light activation of a nontoxic, biologically inert precursor, or photocage, to release a biologically active molecule. While there are no examples of clinically approved photocages, spatiotemporal control of therapeutic delivery has great potential to circumvent off-target toxicity of the photolabile molecule. PDT and PCT involve excitation of the Ru(II) complex from the 1 GS to the singlet metal-to-ligand charge transfer (1 MLCT) state, which undergoes efficient ultrafast intersystem crossing to the corresponding triplet 3 MLCT state. Whereas PDT relies on the presence of a long-lived triplet excited state, $^{3}\pi\pi^*$ or 3 MLCT, to produce reactive 1 O₂, PCT requires access to the dissociative triplet metal-centered (3 MC) excited state, which allows for release of bioactive ligands upon excitation. Ru(II)-based PDT and PCT were thought to be mutually exclusive until the first dual PCT/PDT agent, [Ru(tpy)(Me₂dppn)(py)]²⁺ was reported. Place of 2 1,222 Incorporation of the π -extended ligand 3,6-dimethylbenzo[i]dipyrido[3,2-a:20,30-a]phenazine (Me₂dppn) results in a lowest energy, long-lived dppn-centered $^{3}\pi\pi^*$ state, leading to efficient 1 O₂ production for PDT, while the introduction of methyl groups generates steric strain and distortion

of octahedral geometry, resulting in a low-lying ³MC state that allows pyridine ligand photodissociation.

We previously reported a Ru(II)-based complex 1 shown in Figure 1, which contains an irreversible cathepsin inhibitor and Medppn ligand for the ¹O₂ generation and inhibitor delivery, resulting in the important synergism of PCT/PDT dual-action agents.²³ Cathepsins are essential proteases responsible for protein catabolism and autophagy. In the acidic tumor microenvironment, cathepsins translocate from lysosomes to the cell surface and extracellular milieu and contribute to degradation of the extracellular matrix (ECM), either directly or indirectly through activation of the proteolytic cascade.^{24–27} In fact, overexpression of cathepsins has been associated with poor prognosis of various cancers.^{28,29} Importantly, in vitro studies using cathepsin inhibitors^{30–37} and in vivo studies involving cathepsin gene knockout mice^{38–41} have resulted in decreased tumor burden, invasion, and proliferation. Because cathepsins are well known to reside at the invasive edge of tumors. 42 irreversible inhibition of the cathepsin enzyme provides an anticancer effect that can also serve as a delivery method selective to tumor tissue. Following irreversible, covalent inhibition of cathepsins, light activation allows the photolabile inhibitor to be released from the Ru(II) center, where the solvated Ru(II) complex produces ¹O₂ and induces oxidative damage at the tumor site.²³ This study demonstrated the synergism of simultaneous cathepsin inhibition and ROS generation in a 3D pathomimetic model of triple negative human breast cancer, which offered promise for a drug delivery method, albeit limited by blue-light activation.

Figure 1. Previously reported dual action PCT/PDT agents, cathepsin-based inhibitor **1** (right) reported to show synergistic cell death against breast cancer spheroids and pyridyl photocage **2** (left) reported to show immunogenic cell death in 3D coculture containing macrophages and triple negative breast cancer cells.

Our groups have also reported that dual action PCT/PDT metal complexes such as **2** (Figure 1) show the ability to target MDA-MB-231 triple negative breast cancer cells and tumor-associated macrophages (TAMs).⁴³ Macrophages are myeloid cells responsible for modulating the immune system by phagocytosis, antigen presentation, and secreting cytokines, chemokines, and growth factors. To mediate the immune system, these cells must be adaptable to the tissue they reside in and to the environmental cues, therefore, macrophages differentiate across a spectrum between pro-inflammatory, immune activating M1 macrophages or anti-inflammatory, immune suppressing M2 macrophages.^{44–47} Studies have indicated that tumor regression caused by cathepsin inhibitors may be due to depletion of TAMs or repolarization towards M1-like macrophages.^{30,48–51} While our lead compound **2** showed efficacy against macrophages and promise for metal-based immunotherapy, we predicted it would lack specificity if applied *in vivo*. Thus, we envisioned implementing a metal-based cathepsin inhibitor to not only direct the compound to tumor cells, but also TAMs. Together, we hypothesized that appending a cathepsin inhibitor to a green light

activated PCT/PDT agent would aid delivery to the tumor microenvironment and immunogenic response with improved tissue penetration.

Herein, we report the design, synthesis, and biological evaluation of a Ru(II)-containing photolabile cathepsin inhibitor. While many photoactivated Ru(II) complexes have been designed to display red-shifted absorption windows with high extinction coefficients, they generally feature π -extended ligands that reduce their solubility in aqueous media, organic chromophores that are responsible for its photosensitization properties, or nanoparticles that incorporate many Ru(II) molecules. Moreover, in attempts to shift Ru(II) complexes to the therapeutic window, the PCT mode is sacrificed for PDT capabilities, therefore only a handful of dual PCT/PDT agents can be activated with green or red light. 52-57 In our synthetic design, we utilized an intermediate aldehyde that can be subjected to facile oxime formation via a "click" reaction to efficiently produce conjugates with green light activated dual action PCT/PDT analogs.⁵⁸ The Ru PCT/PDT-cathepsin inhibitor conjugate prepared by this method efficiently inactivates purified cathepsins B and L in both upon irradiation and when kept in the dark. Furthermore, cathepsin inactivation was evident in cells treated with our compound, thereby confirming cellular uptake and inactivation of intracellular cysteine cathepsins. Photoactivation with green light results in photorelease of the inhibitor conjugate and phototoxicity in breast cancer cells and macrophages using short intervals of irradiation, which shows promise for further biological applications. Importantly, we demonstrate that conjugation to a cathepsin inhibitor can be used to mitigate toxicity of Ru PCT/PDT agents in the dark.

Results and Discussion

Compound Design

We hypothesized that designing a Ru(II) complex that contains both PDT and PCT modalities in addition to a cathepsin inhibitor would enable specific targeting to the tumor region where these enzymes are overexpressed. In this scenario, the covalent inhibition of cathepsins would allow for localization of the Ru(II) complex at the invasive tumor edge, where cathepsins are known to be found. Following localization, the release of the covalently bound inhibitor from the Ru(II) center and ROS production can then be achieved through the irradiation of the complex with visible light, resulting in oxidative damage to TAMs and tumor cells. We previously reported a Ru PCT/PDT agent conjugated to a cathepsin inhibitor, where the dual action PCT/PDT behavior was crucial for achieving photoactivated cell death. However, our previously reported complexes were only photoactivatable upon blue light irradiation with low tissue penetration depth, thereby limiting their potential biological applications. Here, we have designed a dual PCT/PDT Ru(II)-cathepsin inhibitor that employs green light activation, which penetrates tissue deeper than blue light and has clinically validated applications in PDT. 59,60

To ensure our Ru(II) complex could be activated by green light and serve as PDT agent, ancillary ligands were chosen to move absorption to longer wavelengths, as well as to optimize cellular penetration and $^{1}O_{2}$ production. Ru(II) complexes containing benzo[i]-dipyrido[3,2-a:2',3'-c]phenazine (dppn) ligands have been proven to elicit efficient PDT achieved by its lowest-energy, long-lived dppn-centered $^{3}\pi\pi^{*}$ excited state. Additionally, inclusion of the more extended π -system in 2,6-di(quinoline-2-yl)pyridine (dqpy) has been shown to result in a red shift of the 1 MLCT absorption as compared to the traditional tridentate terpyridine (tpy) ligand. Incorporation of these ligands in [Ru(dppn)(dqpy)(py)](PF₆)₂ indeed showed phototoxicity using green light (520-525nm) in a preliminary screen (data not shown), indicating the parent complex serves as a promising PDT agent.

Because in dppn-containing complexes PDT arises from thermal population of the lowest-lying ${}^3\pi\pi^*$ state from the ${}^3\text{MLCT}$, this process is generally more favorable than population of the higher-energy dissociative ${}^3\text{MC}$ state required for PCT. To make PCT a feasible process, we appended a less basic and weaker monodentate ligand, 1H-1,2,4-triazole, to serve as the photolabile ligand. To allow for cathepsin inhibition in both the dark and light, the photolabile ligand was designed to contain an epoxysuccinyl group found in commonly known cathepsin inhibitors CA-074, E64d, and NS-134. The epoxysuccinyl warhead enables irreversible inhibition *via* epoxide opening by the cysteine of the cathepsin. Additionally, while it is known that CA-074 is cell impermeable, its methyl ester analog CA-074Me (Figure 2) behaves as a cell permeable prodrug that it is hydrolyzed to CA-074 by intracellular esterases. ${}^{64-66}$ Thus, we sought to conserve the terminal ester of the inhibitor conjugate to allow for cell permeability and inhibition of intracellular cathepsins.

Figure 2. Cell permeable cathepsin inhibitors, CA-074Me and E64d.

Due to forcing conditions required to complex the weak triazole ligand to the Ru(II) center and opposing lability of the epoxide group, we employed a "click" reaction, where we could separately complex triazole and subsequently attach the epoxysuccinyl warhead. The synthesis of the terminal benzaldehyde intermediate (5) allowed for a facile oxime reaction commonly found in bioconjugation reactions where hydroxylamines can "click" with aldehydes or ketones to generate a stable oxime.^{67–72} Additionally, the hydroxylamine precursor (8) contained a diethylene

chain to aid in water solubility and lengthen the linker between the Ru(II) center and the epoxysuccinyl warhead to allow for covalent binding to the active site under dark conditions. In addition to our Ru(II)-based cathepsin inhibitor, we also synthesized a Ru(II) complex containing an identical core devoid of the inhibitor conjugate, $[Ru(dqpy)(dppn)(MeTz)]^{2+}$ where MeTz = 1-methyl-1H-1,2,4-triazole (6). We hypothesized that 6 would also be phototoxic due to its PDT properties, however due to the absence of the cathepsin inhibitor it lacks the drug delivery vector.

Compound Synthesis & Structural Characterization Data

Because triazole is a weak ligand, forcing conditions such as high temperatures and excess ligand were necessary to complex the triazole ligand to ruthenium. To prevent decomposition of our labile epoxysuccinyl containing ligand, we synthesized our target Ru(II)-based inhibitor in several steps, as depicted in Scheme 1. A terminal benzaldehyde motif was incorporated to carry out the oxime reaction. We first attempted to synthesize 4-((1*H*-1,2,4-triazol-1-yl)methyl)benzaldehyde, however unwanted side reactions occurred upon complexation to ruthenium, presumably due to activation of the aldehyde carbonyl group. Instead, we used acetal protected 1-(chloromethyl)-4-(diethoxymethyl)benzene and substituted the chloride for 1*H*-1,2,4-triazole in the presence of catalytic NaI and K₂CO₃ to give 3.

Before complexing triazole to ruthenium, we first constructed our precursor ruthenium complex. To make [Ru(dppn)(dqpy)(Cl)]PF₆ (4), we synthesized [Ru(dppn)(*p*-cymene)Cl]Cl according to the literature,⁷³ and subjected it to two equivalents of dqpy ligand and excess LiCl in DMF at reflux, during which the color changed from orange to purple. Electronic absorption spectroscopy revealed a red-shift of the ¹MLCT band from the starting material at 419 nm to 535 nm for the product,⁷³ indicating successful complexation. The purple solid was isolated *via* NH₄PF₆ precipitation and alumina column chromatography. The complex was then subjected to

AgBF₄ in 1:1 DCM:MeOH to exchange the chloride for a more labile leaving group. The reaction mixture was filtered to remove AgCl, concentrated, and refluxed in 2:1 ethylene glycol:EtOH with excess triazole-containing ligand (3). Isolation by NH₄PF₆ precipitation and subsequent vapor diffusion using acetonitrile and Et₂O serendipitously afforded the deprotected aldehyde 5. Hydrolysis of the acetal presumably occurred due to adventitious water in the medium. The control compound 6 was synthesized in a similar fashion containing a methyl group rather than a benzaldehyde motif for conjugation using 1-methyl-1*H*-1,2,4-triazole as the ligand. Analysis by electronic absorption spectroscopy of both complexation reactions displayed a MLCT shift to 470 nm demonstrating the reaction was successful.

Scheme 1. A) Synthesis of triazole-containing acetal, **3**. B) Synthesis of Ru(II)-containing aldehyde, **5**, and control compound, **6**.

In order to generate the hydroxylamine portion for the desired oxime reaction, we first attached the hydroxylamine to an ethylene glycol linker. Monocoupling of 2-(((tertbutoxycarbonyl)amino)oxy)acetic acid with 2,2'-(ethylenedioxy)bis(ethylamine) with DCC as a coupling agent afforded 7 (Scheme 2). Subsequent coupling of the terminal amine with 4nitrophenyl (tert-butoxycarbonyl)-L-leucinate gave the leucine containing Boc-protected hydroxylamine, 8, as shown in Scheme 2. To make the hydroxylamine accessible, the ligand was treated with 1 M HCl to deprotect both Boc groups. The HCl salt intermediate was added in excess to the ruthenium-containing aldehyde 5 and was isolated via NH₄PF₆ precipitation and EtOAc trituration to remove the unreacted ligand (Scheme 2). The successful oxime reaction was validated by ESI/MS analysis displaying the m/z value of 636 and ¹H-NMR revealed a new proton signal belonging to the oxime proton at 8.23 ppm and simultaneous disappearance of the aldehyde proton. Additionally, no evidence of imine formation from the terminal amine and aldehyde was found, where the chemical shift of the imine hydrogen would be expected at ~8.1 ppm. This observation is consistent with prior reports indicating that imine formation is fast and reversible, whereas oximes are more thermodynamically stable. 70–72

Scheme 2. Synthesis of Ru(II) PCT/PDT-cathepsin inhibitor conjugate **9**.

As shown in Scheme 2, the oxime was treated with excess 2-ethyl 3-(4-nitrophenyl) (2S,3S)-oxirane-2,3-dicarboxylate and DIPEA to attach the epoxide-containing activated ester to the leucyl-amine to give final compound **9**. This specific epoxide group was chosen in **9** to generate an analog of E64d, a pan-cathepsin inhibitor with affinity for cathepsins B and L, two prominent cysteine proteases found in the tumor microenvironment.⁷⁴ High resolution ESI/MS analysis showed the correct m/z value of 706.2241 as well as the expected isotopic distribution (Figure S8). Additionally, ¹H-NMR analysis depicted a shift of the α -proton of the leucine residue to 4.43 ppm, revealing successful coupling. While chemical and photochemical analysis was carried out with

the complexes as PF₆⁻ salts, PF₆⁻ anions were exchanged for more the water-soluble Cl⁻ counteranion in complexes **6** and **9** before biological evaluation. The anion exchange was accomplished by dissolving the PF₆⁻ salt of each complex in CH₃CN, adding Amberlite IRA-410(Cl) exchange resin, stirring for 10 min, then filtering. Condensing the filtrate yielded the Cl⁻ salt as verified by the absence of the peak corresponding to the PF₆⁻ counteranion in the ¹⁹F-NMR spectrum.

Photophysical Properties and Photochemistry

The ground- and excited-state properties of the inhibitor-containing Ru(II) complex 9 and the control 6 were investigated, and each complex was evaluated for singlet oxygen production and ligand exchange upon irradiation. The absorption spectra of 6 and 9 in CH₃CN are nearly identical in the 350 nm to 700 nm range and are shown in Figure 3a. Complex 6 exhibits a broad peak at 471 nm ($\varepsilon = 8,900 \text{ M}^{-1}\text{cm}^{-1}$) and shoulder at 501 nm ($\varepsilon \sim 8,200 \text{ M}^{-1}\text{cm}^{-1}$) that arise from Ru(II) \rightarrow dppn and Ru(II) \rightarrow dqpy ¹MLCT transitions, respectively. These assignments were made from comparison to related complexes. For example, [Ru(dqpy)(phen)(CH₃CN)]²⁺ (phen = 1,10-phenantholine) features a broad peak at 469 nm ($\varepsilon = 7,900 \text{ M}^{-1}\text{cm}^{-1}$), attributed to the Ru(II) \rightarrow dqpy ¹MLCT transition,⁷⁵ since it is red-shifted relative to the Ru(II) \rightarrow tpy ¹MLCT absorption maximum in [Ru(tpy)(phen)(CH₃CN)]²⁺ at 455 nm ($\varepsilon = 11,000 \text{ M}^{-1}\text{cm}^{-1}$). ⁷⁶ The red-shift in the Ru(II) \rightarrow dqpy ¹MLCT maximum in 6 relative to that in [Ru(dqpy)(phen)(CH₃CN)]²⁺ points at a MeTz serving as a weaker π -acceptor than CH₃CN for π -backbonding, resulting in a lower amount of stabilization of the t_{2g}-type d-orbital set and a smaller energy gap between the metal-centered highest occupied molecular orbitals (HOMOs) and the dqpy(π *) lowest

unoccupied orbital (LUMO), since the energy of the latter is expected to remain relatively constant in these complexes. In addition, two lower energy Ru(II) \rightarrow dqpy 1 MLCT bands are observed for [Ru(dqpy)(phen)(CH₃CN)] $^{2+}$ at 534 nm (ϵ = 2,300 M $^{-1}$ cm $^{-1}$) and 600 nm (ϵ = 1,100 M $^{-1}$ cm $^{-1}$), which appear at 580 nm (ϵ = 2,600 M $^{-1}$ cm $^{-1}$) and 640 nm (ϵ = 1,200 M $^{-1}$ cm $^{-1}$) in **6**. The absorption spectrum of **6** also features strong dppn-centered $^{1}\pi\pi^*$ absorption at 408 nm (ϵ = 10,000 M $^{-1}$ cm $^{-1}$), also present in other Ru(II) complexes with dppn ligands. 21,61 In addition, **6** features a sharp peak at 373 nm (ϵ = 24,000 M $^{-1}$ cm $^{-1}$) that is not observed in [Ru(dqpy)(phen)(CH₃CN)] $^{2+}$ or [Ru(dqpy)(dppn)(CH₃CN)] $^{2+}$, such that it has been assigned as arising from a transition involving the MeTz ligand.

The transient absorption spectra of **6** and **9** collected in deareated acetone following 532 nm (fwhm ~ 8 ns) excitation exhibit a broad positive signal in the 500 – 600 nm range with maximum at ~ 540 nm, shown for **9** in Figure 3b. The signal at 540 nm for each complex can be fitted to a monoexponential function resulting in lifetimes, τ , of 3.8 μ s and 8.5 μ s for **6** and **9**, respectively. The peak at ~ 540 nm and its long lifetime are consistent with a $^3\pi\pi^*$ excited state localized on the dppn ligand, as previously reported for related complexes with a dppn ligand.

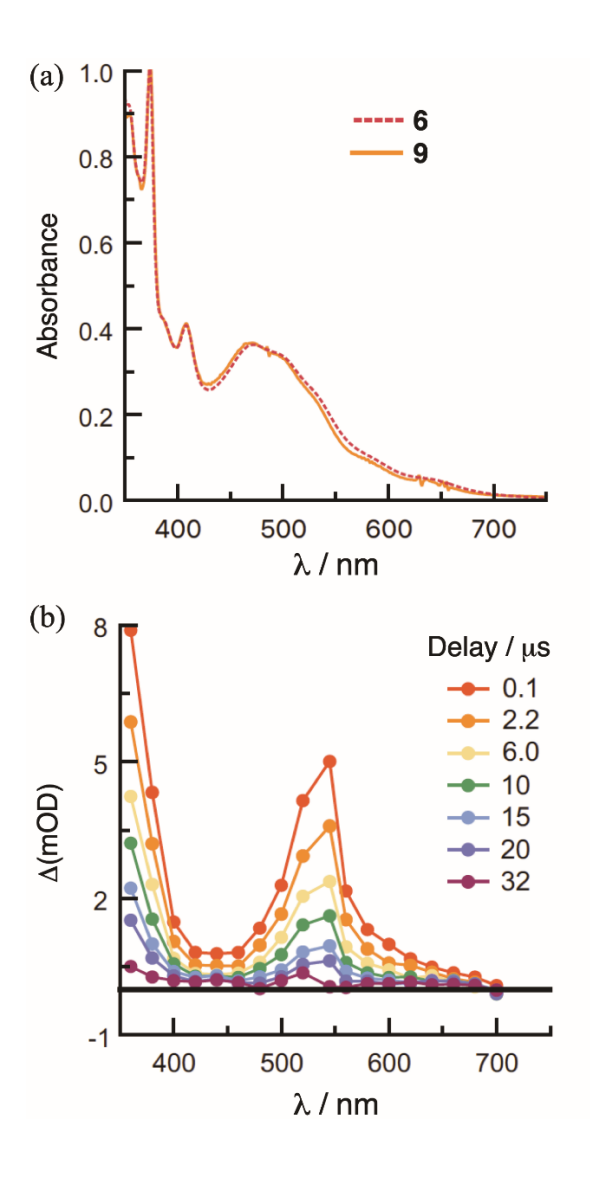


Figure 3. (a) Electronic absorption spectra of **6** and **9** in CH₃CN and (b) transient absorption spectra of **9** in acetone recorded at various delay times following a 532 nm (fwhm ~ 8 ns) laser pulse under N₂.

Upon steady-state irradiation in ambient conditions, complexes **6** and **9** produce ${}^{1}O_{2}$ with quantum yields, Φ_{Δ} , of 0.78(4) and 0.8(1), respectively, in methanol ($\lambda_{irr} = 460$ nm). In addition, under a nitrogen atmosphere to prevent the formation of ${}^{1}O_{2}$, the photolysis of **6** and **9** result in the exchange of triazole ligand for a solvent CH₃CN molecule, as shown in Figure 4 for **6**. It is evident from Figure 4 that there are isosbestic points at 240 nm, 275 nm, 293 nm, 481 nm, and 503 nm,

indicating the clean conversion from the starting material to the solvated product, $[Ru(dqpy)(dppn)(CH_3CN)]^{2+}$. In addition, the maxima of the product are consistent with those previously reported for the related complex $[Ru(dqpy)(phen)(CH_3CN)]^{2+}$. It should be noted that the peak at 373 nm associated with the MeTz ligand decreases in intensity during photolysis, consistent with the exchange of the monodentate ligand for a solvent molecule. The release of MeTz ligand was also confirmed by monitoring photolysis of 9 by ¹H-NMR spectroscopy (Figure S22.) The quantum yields for MeTz ligand exchange upon 500 nm irradiation, Φ_{500} , of 6 and 9 were determined to be 0.025(8) and 0.008(2), respectively, in CH₃CN.

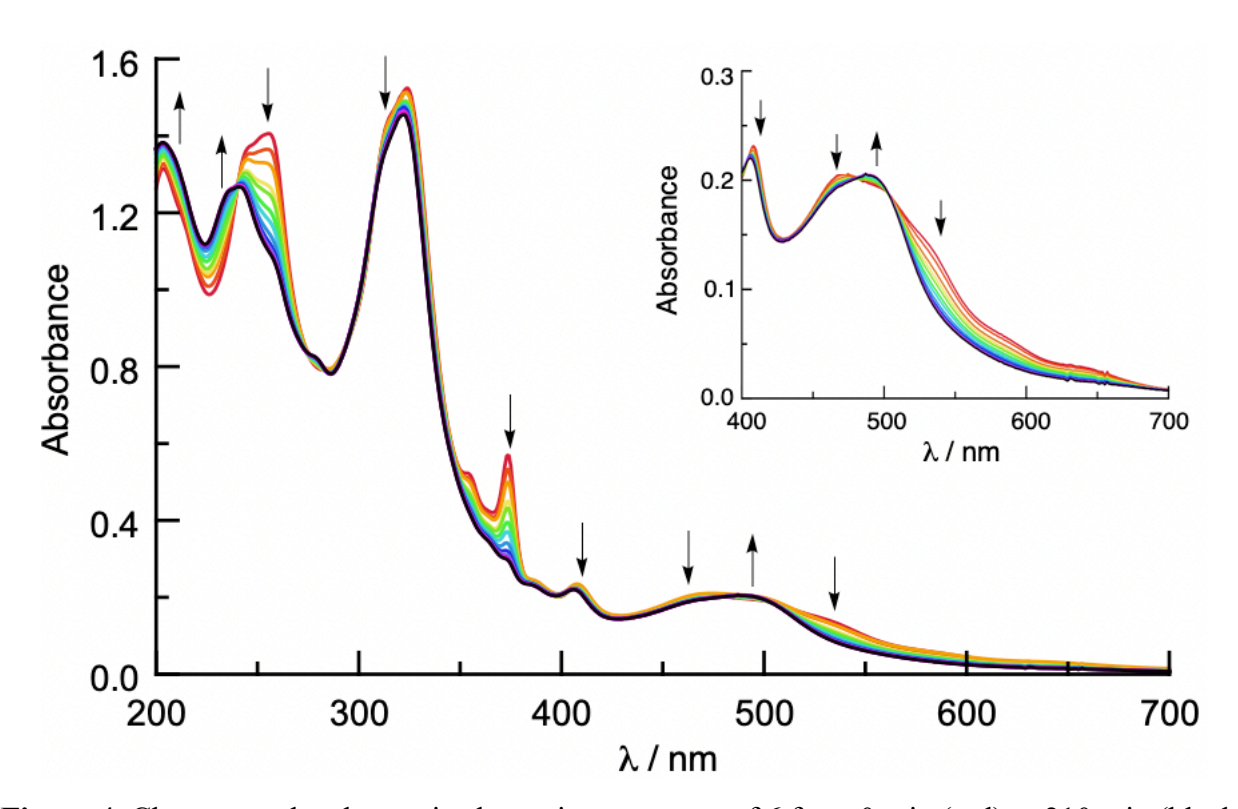


Figure 4. Changes to the electronic absorption spectrum of **6** from 0 min (red) to 210 min (black) upon 670 nm irradiation in CH₃CN (Inset: expanded view of the visible range).

Complex Stability & Distribution Coefficients

Before proceeding to biological evaluation of complexes **6** and **9**, preliminary studies were pursued to confirm complex stability and gain insight of its potential ability to penetrate cells. Stock solutions of complexes **6** and **9** in DMSO were diluted in cell growth media (RPMI 1640, containing 10% FBS) at 37 °C and monitored in the dark over the course of 24 h by electronic absorption spectroscopy (Figures S20-21). While reduction in overall absorbance was noted over time, presumably due to aggregation, no spectral shifts in the MLCT bands indicating release of the triazole ligand were detected.

To further predict how complexes 6 and 9 would behave in cells, the distribution coefficient was determined to estimate their ability to penetrate cellular membranes. A positive distribution coefficient value is generally desired, usually indicating the compound is lipophilic and can cross the cell membrane. While Ru(II) complexes can show enhanced cellular uptake due to their lipophilic cationic nature, lipophilicity characteristics can vary among complexes leading to differences in cellular permeability. In our case, ligands dqpy and dppn are highly lipophilic and presented solubility issues during synthesis, thus it was crucial to offset this lipophilicity to ensure solubility in aqueous cell growth media, while maintaining feasible cell permeability. The distribution coefficient of the inhibitor Ru(II) complex 9 and of the control compound 6 were found to be 0.05 ± 0.01 and -0.26 ± 0.02 , respectively, using the "Shake-Flask" method. Despite the lipophilic ligands present in both complexes, it is evident that the hydrophilic nature of 6 can be attributed to its overall 2+ charge. While the inhibitor complex 9 contains more hydrogen-bond donors, it was slightly more lipophilic than 6, presumably due to the presence of the benzyl group or leucine side chain. Nonetheless, lipophilicity is desirable to allow for permeation of the cell membrane. It was also hypothesized that the presence of the ester in 9 would aid in cellular uptake and retention, similar to ester CA-074Me that undergoes cellular uptake, followed by cleavage from intracellular esterases to form the carboxylate product CA-074 that is not cell permeable.⁶⁴

Cathepsin B and L Inhibition

To evaluate the ability of the inhibitor conjugate of compound 9 to inactivate cysteine cathepsins and serve as a delivery vector to TAMs and tumor cells, we measured its inhibitory properties using a purified enzyme assay. We chose to study inhibition of cathepsins B (CTSB) and L (CTSL) specifically for their relevance in cancer. ^{40,77–79} Fluorogenic substrates (100 μM), Z-Arg-Arg-AMC (CTSB) or Z-Phe-Arg-AMC (CTSL) and varying concentrations of complex 7 $(0.05 \text{ to } 0.30 \mu\text{M} \text{ final}) \text{ or } 4 (0.5 \text{ to } 25 \mu\text{M} \text{ final}) \text{ were treated with green light } (520-525 \text{ nm}) \text{ for } 10$ min or left in the dark. Activated CTSB or CTSL was added, and the activity was immediately monitored by following the formation of the hydrolyzed, fluorescent 7-amino-4-methylcoumarin (AMC) product. Data were fit to a two-step model for irreversible inhibition (Figure S12), which provided the quotient k_{inact}/K_i representing the second-order rate constant for enzyme inactivation, that includes covalent bond formation via epoxide opening. Compound 9 successfully inhibited CTSB and CTSL under light and dark conditions with k_{inact}/K_i values within error (0.8 to 3 × 10⁴ M^{-1} s⁻¹) (Table 1, Figure S14). Furthermore, we found that the control complex 6 was unable to inhibit CTSB or CTSL in dark or upon irradiation at concentrations as high as 25 μM (Figure S15). This result shows that the epoxysuccinyl warhead is crucial for irreversible cathepsin inhibition, rather than the cysteine active site thiolate binding to the open coordination site of the metal following triazole photorelease, which has been reported as a mechanism of cysteine protease inhibition by Ru(II) complexes. 80,81

Table 1. Second order rate constants, k_{inact}/K_i (M⁻¹ s⁻¹), for CTSB and CTSL inactivation.

	C	TSB^a	CTSL^b		
Compound	Dark	Light	Dark	Light	
6	<10	<10	<10	<10	
9	$3 \pm 2 \times 10^4$	$9.4 \pm 0.3 \times 10^3$	$8 \pm 2 \times 10^3$	$9 \pm 2 \times 10^{3}$	

"Conditions: The CTSB stock was diluted to 16 nM (4 nM final concentration) in assay buffer (0.4 M acetate, pH 5.5, 5 mM EDTA, 0.01% Triton X-100) containing 8 mM DTT. Inhibitors were prepared as <1% DMSO stock solutions in assay buffer to achieve final concentrations ranging from 0.30 to 0.05 μM for 9 and 25 to 0.5 μM for 6. Complexes 6 and 9 were irradiated with green (520-25 nm) light (t_{irr} = 10 min) or left in the dark. The substrate Z-Arg-AMC in assay buffer (200 μM, 50 μL) was diluted to achieve a final concentration of 100 μM. CA-074 was used as a positive control for cathepsin B inhibition. Fluorescent readings (λ_{ex} = 360nm, λ_{em} = 430 nm, 5 flashes/well) were immediately taken every 30 s for 15 min at room temperature. b CSTL assay was carried out analogously, however in 0.4 M acetate buffer, 4 mM EDTA, pH 5.5, 0.01% Triton X-100 with substrate Z-Phe-Arg-AMC. Data was fit to a two-step model for irreversible inhibition using DynaFit, which provided the quotient k_{inact}/K_i .

Confirmed inhibition of isolated CTSB and CTSL supported the idea that 9 should be able to inhibit cathepsins secreted into the extracellular milieu, commonly found in the tumor microenvironment. To further investigate the ability of 9 to inhibit intracellular cathepsins, we treated cancer cells with 6 or 9 then examined cathepsin inhibition in cell lysates. Murine breast cancer 4T1 cells were chosen to investigate biological properties of 6 and 9 to ensure data collected would be informative for future experiments using syngeneic mice models to measure immunogenic effects. 4T1 cells were treated with vehicle or 1 µM of known, permeable cathepsin inhibitor E64d as a positive control, 6, or 9. After 4 h incubation, cell growth media was replaced with fresh media to remove impermeable compounds. The cells were then irradiated or left in the dark for 10 min, and then incubated for 1 h. Next, the media was aspirated, and the cells were washed with PBS and lysed. Lysates were diluted and activated with assay buffer and fluorogenic

substrate was added. Again, cathepsin inhibition was monitored by a progression curve related to hydrolysis, and formation of fluorescent AMC. It is important to note that Z-Arg-Arg-AMC is a selective substrate for CTSB, whereas Z-Phe-Arg-AMC lacks high selectivity towards CTSL, thus inhibition of Z-Phe-Arg-AMC hydrolysis shows more general cathepsin inhibition. Collectively, these studies demonstrated that complex 9 can indeed inactivate intracellular cathepsins both under visible light irradiation and in the dark at concentrations as low as 1 μM (Table 2, Figure S18-19). Additionally, complex 6 showed no significant inhibition except under light conditions with substrate Z-Arg-AmC, presumably due to ROS generation which either directly or indirectly led to loss of cathepsin B activity. Effective inhibition of intracellular cathepsins also supports the hypothesis that complex 9 can penetrate the cells and behave as delivery vector to cancer and stromal cells in the tumor microenvironment where cysteine cathepsins are overexpressed.

Table 2. Percent activity of cysteine cathepsins in 4T1 cells treated with E64d, **6** or **9** using substrates Z-Arg-Arg-AMC or Z-Phe-Arg-AMC.

	Substrate Z-Arg-Arg-AMC		Substrate Z-Phe-Arg-AMC		
Compound	Light	Dark	Light	Dark	
E64d	<5	<5	21 ± 4	18 ± 4	
6	53 ± 8	118 ± 4	110 ± 16	94 ± 8	
9	<5	<5	6 ± 2	6 ± 2	

 $^{^{\}alpha}$ Conditions: 4T1 cells were treated with vehicle or 1 μM E64d, 6, or 9, incubated for 4 h, irradiated with green (520-25 nm) light (t_{irr} = 10 min) or left in the dark, and then incubated for an additional hour before lysing. Pretreated cell lysates were diluted in assay buffer (0.4 M acetate, pH 5.5, 5 mM EDTA, 0.01% Triton X-100) containing 8 mM DTT. Following activation of lysates for 10 min at 37°C, lysates were diluted 2x with 200 μM substrate Z-Arg-Arg-AMC or Z-Phe-Arg-AMC,

to give final concentration 100 μ M. Fluorescent readings ($\lambda_{ex} = 360$ nm, $\lambda_{em} = 430$ nm, 5 flashes/well) were immediately taken every 30 s for 5 min at 37°C. Percent activities were determined relative to the vehicle control.

Cellular Studies

Following verification of intra- and extracellular cathepsin inhibition, complexes 6 and 9 were evaluated against bone marrow-derived BALB/c M0, M1, and M2 macrophages, 4T1 cells, and murine L929 fibroblasts in 2D culture. The cells were treated with 6 or 9 (0.1 to 18 µM) and incubated for 4 h, after which time the cell growth media was replaced with fresh media and the cells were irradiated with green light (520-525 nm) for 10 min. Cells under dark conditions were treated similarly in the absence of irradiation, however, with a larger range of concentrations (0.1 to 50 µM). After 72 h, cell viability was assessed by MTT assay. As anticipated, both 6 and 9 showed strong phototoxicity due to their ability to produce ROS (Table 3). While 6 and 9 did show undesired phototoxicity in L929 fibroblasts, phototoxicity in normal tissue should be avoided if complexes were irradiated only in cancerous tissue. Moreover, in the same cell line, 6 and 9 displayed EC₅₀ values within error under light conditions, consistent with ¹O₂ generation through energy transfer (PDT mechanism), rather than cathepsin inhibition, driving cell death. Fortunately, appending the inhibitor conjugate in complex 9 ameliorated cellular toxicity found with 6 in the dark. Compound 9 showed excellent photoselectivity with PI values as high as >19 with no evidence of toxicity at concentrations up to 50 µM across all cell lines in the dark; higher concentrations of 9 were not evaluated due to low solubility. In contrast, 6 showed EC₅₀ values ranging from 19-36 μM in the dark in all cell lines tested. Additionally, a ~5-fold higher potency was observed for 9 in macrophages vs. tumor 4T1 cells, consistent with our previously reported compound 2, which was also more potent in macrophages as compared to TNBC cells.⁴³

Importantly, Blum et. al. reported a cathepsin inhibitor that was able to kill macrophage cells *in vitro* and reduce tumor cell mass *in vivo*, however elicited no effect in 4T1 cells grown in 2D.³⁰ This finding suggests that while the complex may not be potent against tumor cells, TAM cell death can induce an immune response and subsequent cell death of neighboring tumor cells when further applied in 3D coculture or *in vivo*.

Table 3. EC₅₀ values (μ M) and phototherapeutic indexes (PI) of **6** and **9** in murine macrophage (M0, M1, M2), triple negative breast cancer (4T1) and fibroblast (L929) cell lines.^a

	Compound 6			Compound 9		
Cell line	Light EC ₅₀	Dark EC ₅₀	ΡI	Light EC ₅₀	Dark EC ₅₀	PI
M0	2.0 ± 0.6	20 ± 1	10	2.7 ± 0.6	>50	>19
M1	2.3 ± 0.7	19 ± 1	8	2.9 ± 0.9	>50	>17
M2	2.0 ± 0.3	19 ± 3	10	2.4 ± 0.3	>50	>21
4T1	14 ± 1	30 ± 5	2	15 ± 1	>50	>3
L929	2.6 ± 0.9	36 ± 9	14	3 ± 1	>50	>17

^aCells treated with **6** or **9** for 4 h, treatments were replaced with vehicle, and cells were irradiated with green (520-25 nm) light ($t_{irr} = 10$ min) or left in the dark. Cell viability was determined by MTT assay 72 h after irradiation. Data are the average of three independent experiments using quadruplicate wells, and errors shown are standard deviations. PI = phototherapeutic index = ratio dark EC₅₀/light EC₅₀.

While attachment of the cathepsin inhibitor conjugate did not make 9 more potent than 6, 2D cell culture does not accurately mimic the tumor microenvironment, especially phenotypes where cysteine proteases are translocated to the cell surface and act along the invasive edge of

tumors. Future studies will investigate the biological effect of complex 9 in 3D coculture experiments containing both macrophages and tumor cells. This heterogenous coculture provides a more accurate depiction of the tumor microenvironment, including interactions with the extracellular matrix (ECM), cell polarity, and cell-to-cell contacts. Our previous cathepsin inhibitor 1 (Figure 1) was found to be more toxic in 3D MDA-MB-231 spheroids versus cells grown in 2D, presumably due to greater translocation of cathepsins to the cell surface.²³ Thus, complex 9 has the potential to show additional anti-cancer effects that are not presented in 2D culture. Meanwhile employing green light irradiation is expected to broaden the scope of compounds such as 9 in anti-cancer applications as compared to previous analogs activated with blue light. Finally, our previously reported dual PCT/PDT agent [Ru(tpy)(Me₂dppn)(py)]²⁺ 2 was able to target macrophages and yield an immunogenic response without a method of drug delivery. 43 Therefore inclusion of cathepsin inhibitor to deliver our Ru(II) PCT/PDT agent to TAMs and tumor cells has great potential to show an enhanced immunotherapeutic effect. Activitybased probes activated by cathepsins have shown that cathepsins are highly expressed in cancerous tissues^{82–84} and cathepsin inhibition provides a useful pharmacological effect for inhibiting metastasis and for enhancing drug delivery.85-88

Conclusions

We report the design, synthesis, and biological evaluation of novel Ru(II) PCT/PDT agents. Triazole-containing compounds **6** and **9** were characterized to show photoactivated ligand dissociation and photosensitization of ${}^{1}O_{2}$ for dual action PCT/PDT applications with green light. Importantly, we demonstrate that the Ru PCT/PDT complex **5** containing an aldehyde can be used in an oxime "click" reaction for conjugation to drug delivery vectors to prepare compounds such

as the cathepsin conjugate **9**. Complex **9** is able to inactivate intra- and extracellular cathepsins in the dark and light, for delivery vector applications to macrophages and tumor cells. Additionally, cell viability studies indicated that PDT is the driving force for cell death where complex **6** and **9** show similar efficacy in the light. Fortunately, cathepsin conjugation was able to reduce the toxicity of the Ru PCT/PDT agent in dark for **9** vs the control complex **6**. Importantly previous PCT/PDT agents displayed immunogenic effects in 3D coculture containing macrophages and tumor cells. Thus, conjugate **9** has great potential for metalloimmunotherapy applications. Studies are now underway to evaluate **9** in 3D co-culture and *in vivo* models of breast cancer.

Acknowledgments. We gratefully acknowledge the National Science Foundation (CHE 2102508), National Institute of Health (T32GM142519), and Wayne State University (Grants Boost and Rumle Fellowship to MD) for support of this research. NMR resources are supported by the National Institutes of Health (S10OD028488) and High Resolution Mass Spectrometry Resources are supported by R01 GM098285-07S1.

Supporting Information

The Supporting Information is available free of charge on the internet.

Detailed experimental procedures of synthesis of compounds **6** and **9**, corresponding ¹H NMR spectral data; biological assays (cell viability MTT assay for **6** and **9**; cathepsin inhibition assay in purified enzymes and in 4T1 cell lysates), stability studies of **6** and **9**, photophysical properties of complexes **6** and **9**.

References

- (1) *Cancer*. https://www.who.int/news-room/fact-sheets/detail/cancer (accessed 2024-01-29).
- (2) Siegel, R. L.; Miller, K. D.; Wagle, N. S.; Jemal, A. Cancer Statistics, 2023. *CA Cancer J. Clin.* **2023**, *73* (1), 17–48. https://doi.org/10.3322/caac.21763.
- (3) Juris, A.; Balzani, V.; Barigelletti, F.; Campagna, S.; Belser, P.; Zelewsky, A. V. Ru(II) Polypyridine Complexes Photophysics, Photochemistry, Eletrochemistry, and Chemiluminescence. *Coord. Chem. Rev.* **1988**, *84*, 85–277. https://doi.org/10.1016/0010-8545(88)80032-8.
- (4) Friedman, A. E.; Chambron, J. C.; Sauvage, J. P.; Turro, N. J.; Barton, J. K. A Molecular Light Switch for DNA: Ru(Bpy)2(Dppz)2+. *J. Am. Chem. Soc.* **1990**, *112* (12), 4960–4962. https://doi.org/10.1021/ja00168a052.
- (5) Kumar, C. V.; Barton, J. K.; Turro, N. J. Photophysics of Ruthenium Complexes Bound to Double Helical DNA. *J. Am. Chem. Soc.* **1985**, *107* (19), 5518–5523. https://doi.org/10.1021/ja00305a032.
- Greguric, I.; Aldrich-Wright, J. R.; Collins, J. G. A 1 H NMR Study of the Binding of Δ-[Ru(Phen) $_2$ DPQ] $^{2+}$ to the Hexanucleotide d(GTCGAC) $_2$. Evidence for Intercalation from the Minor Groove. *J. Am. Chem. Soc.* **1997**, *119* (15), 3621–3622. https://doi.org/10.1021/ja9623951.
- (7) Fong, J.; Kasimova, K.; Arenas, Y.; Kaspler, P.; Lazic, S.; Mandel, A.; Lilge, L. A Novel Class of Ruthenium-Based Photosensitizers Effectively Kills in Vitro Cancer Cells and in Vivo Tumors. *Photochem. Photobiol. Sci.* **2015**, *14* (11), 2014–2023. https://doi.org/10.1039/c4pp00438h.
- (8) Kaspler, P.; Lazic, S.; Forward, S.; Arenas, Y.; Mandel, A.; Lilge, L. A Ruthenium(Ii) Based Photosensitizer and Transferrin Complexes Enhance Photo-Physical Properties, Cell Uptake, and Photodynamic Therapy Safety and Efficacy. *Photochem. Photobiol. Sci.* **2016**, *15* (4), 481–495. https://doi.org/10.1039/c5pp00450k.
- (9) Gandosio, A.; Purkait, K.; Gasser, G. Recent Approaches towards the Development of Ru(II) Polypyridyl Complexes for Anticancer Photodynamic Therapy. *Chimia* **2021**, *75* (10), 845. https://doi.org/10.2533/chimia.2021.845.
- (10) Martínez-Alonso, M.; Gasser, G. Ruthenium Polypyridyl Complex-Containing Bioconjugates. *Coord. Chem. Rev.* **2021**, *434*, 213736. https://doi.org/10.1016/j.ccr.2020.213736.
- (11) Wu, Y.; Li, S.; Chen, Y.; He, W.; Guo, Z. Recent Advances in Noble Metal Complex Based Photodynamic Therapy. *Chem. Sci.* **2022**, *13* (18), 5085–5106. https://doi.org/10.1039/D1SC05478C.
- (12) Silva, M. J. S. A.; Vinck, R.; Wang, Y.; Saubaméa, B.; Tharaud, M.; Dominguez-Jurado, E.; Karges, J.; Gois, P. M. P.; Gasser, G. Towards Selective Delivery of a Ruthenium(II)

- Polypyridyl Complex-Containing Bombesin Conjugate into Cancer Cells. *ChemBioChem* **2023**, 24 (4), e202200647. https://doi.org/10.1002/cbic.202200647.
- (13) Raza, A.; Archer, S. A.; Fairbanks, S. D.; Smitten, K. L.; Botchway, S. W.; Thomas, J. A.; MacNeil, S.; Haycock, J. W. A Dinuclear Ruthenium(II) Complex Excited by Near-Infrared Light through Two-Photon Absorption Induces Phototoxicity Deep within Hypoxic Regions of Melanoma Cancer Spheroids. *J. Am. Chem. Soc.* **2020**, *142* (10), 4639–4647. https://doi.org/10.1021/jacs.9b11313.
- (14) Monro, S.; Colón, K. L.; Yin, H.; Roque, J.; Konda, P.; Gujar, S.; Thummel, R. P.; Lilge, L.; Cameron, C. G.; McFarland, S. A. Transition Metal Complexes and Photodynamic Therapy from a Tumor-Centered Approach: Challenges, Opportunities, and Highlights from the Development of TLD1433. *Chem. Rev.* **2019**, *119* (2), 797–828. https://doi.org/10.1021/acs.chemrev.8b00211.
- (15) Cuello-Garibo, J.-A.; Meijer, M. S.; Bonnet, S. To Cage or to Be Caged? The Cytotoxic Species in Ruthenium-Based Photoactivated Chemotherapy Is Not Always the Metal. *Chem. Commun.* **2017**, *53* (50), 6768–6771. https://doi.org/10.1039/C7CC03469E.
- (16) Bonnet, S. Why Develop Photoactivated Chemotherapy? *Dalton Trans.* **2018**, *47* (31), 10330–10343. https://doi.org/10.1039/C8DT01585F.
- (17) Farrer, N. J.; Salassa, L.; Sadler, P. J. Photoactivated Chemotherapy (PACT): The Potential of Excited-State d-Block Metals in Medicine. *Dalton Trans.* **2009**, No. 48, 10690. https://doi.org/10.1039/b917753a.
- (18) Busemann, A.; Flaspohler, I.; Zhou, X.-Q.; Schmidt, C.; Goetzfried, S. K.; van Rixel, V. H. S.; Ott, I.; Siegler, M. A.; Bonnet, S. Ruthenium-Based PACT Agents Based on Bisquinoline Chelates: Synthesis, Photochemistry, and Cytotoxicity. *J. Biol. Inorg. Chem.* **2021**, *26* (6), 667–674. https://doi.org/10.1007/s00775-021-01882-8.
- (19) Mari, C.; Pierroz, V.; Leonidova, A.; Ferrari, S.; Gasser, G. Towards Selective Light-Activated RuII-Based Prodrug Candidates. *Eur. J. Inorg. Chem.* **2015**, *2015* (23), 3879–3891. https://doi.org/10.1002/ejic.201500602.
- (20) Bonnet, S. Ruthenium-Based Photoactivated Chemotherapy. *J. Am. Chem. Soc.* **2023**, *145* (43), 23397–23415. https://doi.org/10.1021/jacs.3c01135.
- (21) Knoll, J. D.; Albani, B. A.; Turro, C. Excited State Investigation of a New Ru(II) Complex for Dual Reactivity with Low Energy Light. *Chem. Commun.* **2015**, *51* (42), 8777–8780. https://doi.org/10.1039/C5CC01865J.
- (22) Knoll, J. D.; Albani, B. A.; Durr, C. B.; Turro, C. Unusually Efficient Pyridine Photodissociation from Ru(II) Complexes with Sterically Bulky Bidentate Ancillary Ligands. *J. Phys. Chem. A* **2014**, *118* (45), 10603–10610. https://doi.org/10.1021/jp5057732.
- (23) Arora, K.; Herroon, M.; Al-Afyouni, M. H.; Toupin, N. P.; Rohrabaugh, T. N.; Loftus, L. M.; Podgorski, I.; Turro, C.; Kodanko, J. J. Catch and Release Photosensitizers: Combining Dual-

- Action Ruthenium Complexes with Protease Inactivation for Targeting Invasive Cancers. *J. Am. Chem. Soc.* **2018**, *140* (43), 14367–14380. https://doi.org/10.1021/jacs.8b08853.
- (24) Brix, K.; Dunkhorst, A.; Mayer, K.; Jordans, S. Cysteine Cathepsins: Cellular Roadmap to Different Functions. *Biochimie* **2008**, *90* (2), 194–207. https://doi.org/10.1016/j.biochi.2007.07.024.
- (25) Fonović, M.; Turk, B. Cysteine Cathepsins and Extracellular Matrix Degradation. *Biochim. Biophys. Acta, Gen. Subj.* **2014**, *1840* (8), 2560–2570. https://doi.org/10.1016/j.bbagen.2014.03.017.
- (26) Mason, S. D.; Joyce, J. A. Proteolytic Networks in Cancer. *Trends Cell Biol.* **2011**, *21* (4), 228–237. https://doi.org/10.1016/j.tcb.2010.12.002.
- (27) Mohamed, M. M.; Sloane, B. F. Multifunctional Enzymes in Cancer. *Nat. Rev. Cancer* **2006**, *6* (10), 764–775. https://doi.org/10.1038/nrc1949.
- (28) Yadati, T.; Houben, T.; Bitorina, A.; Shiri-Sverdlov, R. The Ins and Outs of Cathepsins: Physiological Function and Role in Disease Management. *Cells* **2020**, *9* (7), 1679. https://doi.org/10.3390/cells9071679.
- (29) Rudzińska, M.; Parodi, A.; Soond, S. M.; Vinarov, A. Z.; Korolev, D. O.; Morozov, A. O.; Daglioglu, C.; Tutar, Y.; Zamyatnin, A. A. The Role of Cysteine Cathepsins in Cancer Progression and Drug Resistance. *Int. J. Mol. Sci.* **2019**, *20* (14), 3602. https://doi.org/10.3390/ijms20143602.
- (30) Salpeter, S. J.; Pozniak, Y.; Merquiol, E.; Ben-Nun, Y.; Geiger, T.; Blum, G. A Novel Cysteine Cathepsin Inhibitor Yields Macrophage Cell Death and Mammary Tumor Regression. *Oncogene* **2015**, *34* (50), 6066–6078. https://doi.org/10.1038/onc.2015.51.
- (31) Bell-McGuinn, K. M.; Garfall, A. L.; Bogyo, M.; Hanahan, D.; Joyce, J. A. Inhibition of Cysteine Cathepsin Protease Activity Enhances Chemotherapy Regimens by Decreasing Tumor Growth and Invasiveness in a Mouse Model of Multistage Cancer. *Cancer Res.* **2007**, *67* (15), 7378–7385. https://doi.org/10.1158/0008-5472.CAN-07-0602.
- (32) Withana, N. P.; Blum, G.; Sameni, M.; Slaney, C.; Anbalagan, A.; Olive, M. B.; Bidwell, B. N.; Edgington, L.; Wang, L.; Moin, K.; Sloane, B. F.; Anderson, R. L.; Bogyo, M. S.; Parker, B. S. Cathepsin B Inhibition Limits Bone Metastasis in Breast Cancer. *Cancer Res.* **2012**, *72* (5), 1199–1209. https://doi.org/10.1158/0008-5472.CAN-11-2759.
- (33) Elie, B. T.; Gocheva, V.; Shree, T.; Dalrymple, S. A.; Holsinger, L. J.; Joyce, J. A. Identification and Pre-Clinical Testing of a Reversible Cathepsin Protease Inhibitor Reveals Anti-Tumor Efficacy in a Pancreatic Cancer Model. *Biochimie* **2010**, *92* (11), 1618–1624. https://doi.org/10.1016/j.biochi.2010.04.023.
- (34) Shree, T.; Olson, O. C.; Elie, B. T.; Kester, J. C.; Garfall, A. L.; Simpson, K.; Bell-McGuinn, K. M.; Zabor, E. C.; Brogi, E.; Joyce, J. A. Macrophages and Cathepsin Proteases Blunt Chemotherapeutic Response in Breast Cancer. *Genes Dev.* **2011**, *25* (23), 2465–2479. https://doi.org/10.1101/gad.180331.111.

- (35) Premzl, A.; Zavašnik-Bergant, V.; Turk, V.; Kos, J. Intracellular and Extracellular Cathepsin B Facilitate Invasion of MCF-10A neoT Cells through Reconstituted Extracellular Matrix in Vitro. *Exp. Cell Res.* **2003**, *283* (2), 206–214. https://doi.org/10.1016/S0014-4827(02)00055-1.
- (36) Sever, N.; Filipic, M.; Brzin, J.; Lah, T. T. Effect of Cysteine Proteinase Inhibitors on Murine B16 Melanoma Cell Invasion in Vitro. *Biol. Chem.* **2002**, *383* (5), 839–842. https://doi.org/10.1515/BC.2002.088.
- (37) Matarrese, P.; Ascione, B.; Ciarlo, L.; Vona, R.; Leonetti, C.; Scarsella, M.; Mileo, A. M.; Catricalà, C.; Paggi, M. G.; Malorni, W. Cathepsin B Inhibition Interferes with Metastatic Potential of Human Melanoma: An in Vitro and in Vivo Study. *Mol. Cancer* **2010**, *9* (1), 207. https://doi.org/10.1186/1476-4598-9-207.
- (38) Sevenich, L.; Schurigt, U.; Sachse, K.; Gajda, M.; Werner, F.; Müller, S.; Vasiljeva, O.; Schwinde, A.; Klemm, N.; Deussing, J.; Peters, C.; Reinheckel, T. Synergistic Antitumor Effects of Combined Cathepsin B and Cathepsin Z Deficiencies on Breast Cancer Progression and Metastasis in Mice. *Proc. Natl. Acad. Sci. U.S.A.* **2010**, *107* (6), 2497–2502. https://doi.org/10.1073/pnas.0907240107.
- (39) Vasiljeva, O.; Korovin, M.; Gajda, M.; Brodoefel, H.; Bojič, L.; Krüger, A.; Schurigt, U.; Sevenich, L.; Turk, B.; Peters, C.; Reinheckel, T. Reduced Tumour Cell Proliferation and Delayed Development of High-Grade Mammary Carcinomas in Cathepsin B-Deficient Mice. *Oncogene* **2008**, *27* (30), 4191–4199. https://doi.org/10.1038/onc.2008.59.
- (40) Gocheva, V.; Zeng, W.; Ke, D.; Klimstra, D.; Reinheckel, T.; Peters, C.; Hanahan, D.; Joyce, J. A. Distinct Roles for Cysteine Cathepsin Genes in Multistage Tumorigenesis. *Genes Dev.* **2006**, *20* (5), 543–556. https://doi.org/10.1101/gad.1407406.
- (41) Ruffell, B.; Affara, N. I.; Cottone, L.; Junankar, S.; Johansson, M.; DeNardo, D. G.; Korets, L.; Reinheckel, T.; Sloane, B. F.; Bogyo, M.; Coussens, L. M. Cathepsin C Is a Tissue-Specific Regulator of Squamous Carcinogenesis. *Genes Dev.* **2013**, *27* (19), 2086–2098. https://doi.org/10.1101/gad.224899.113.
- (42) Rothberg, J. M.; Bailey, K. M.; Wojtkowiak, J. W.; Ben-Nun, Y.; Bogyo, M.; Weber, E.; Moin, K.; Blum, G.; Mattingly, R. R.; Gillies, R. J.; Sloane, B. F. Acid-Mediated Tumor Proteolysis: Contribution of Cysteine Cathepsins. *Neoplasia* **2013**, *15* (10), 1125-IN9. https://doi.org/10.1593/neo.13946.
- (43) Toupin, N.; Herroon, M. K.; Thummel, R. P.; Turro, C.; Podgorski, I.; Gibson, H.; Kodanko, J. J. Metalloimmunotherapy with Rhodium and Ruthenium Complexes: Targeting Tumor-Associated Macrophages. *Chem. Eur. J.* **2022**, *28* (24). https://doi.org/10.1002/chem.202104430.
- (44) Lendeckel, U.; Venz, S.; Wolke, C. Macrophages: Shapes and Functions. *ChemTexts* **2022**, 8 (2), 12. https://doi.org/10.1007/s40828-022-00163-4.

- (45) Hirayama, D.; Iida, T.; Nakase, H. The Phagocytic Function of Macrophage-Enforcing Innate Immunity and Tissue Homeostasis. *Int. J. Mol. Sci.* **2017**, *19* (1), 92. https://doi.org/10.3390/ijms19010092.
- (46) Shapouri-Moghaddam, A.; Mohammadian, S.; Vazini, H.; Taghadosi, M.; Esmaeili, S.; Mardani, F.; Seifi, B.; Mohammadi, A.; Afshari, J. T.; Sahebkar, A. Macrophage Plasticity, Polarization, and Function in Health and Disease. *J. Cell. Physiol.* **2018**, *233* (9), 6425–6440. https://doi.org/10.1002/jcp.26429.
- (47) Ricketts, T. D.; Prieto-Dominguez, N.; Gowda, P. S.; Ubil, E. Mechanisms of Macrophage Plasticity in the Tumor Environment: Manipulating Activation State to Improve Outcomes. *Front. Immunol.* **2021**, *12*, 642285. https://doi.org/10.3389/fimmu.2021.642285.
- (48) Yang, M.; Liu, J.; Shao, J.; Qin, Y.; Ji, Q.; Zhang, X.; Du, J. Cathepsin S-Mediated Autophagic Flux in Tumor-Associated Macrophages Accelerate Tumor Development by Promoting M2 Polarization. *Mol. Cancer* **2014**, *13* (1), 43. https://doi.org/10.1186/1476-4598-13-43.
- (49) Alam, S.; Liu, Q.; Liu, S.; Liu, Y.; Zhang, Y.; Yang, X.; Liu, G.; Fan, K.; Ma, J. Up-Regulated Cathepsin C Induces Macrophage M1 Polarization through FAK-Triggered P38 MAPK/NF-κB Pathway. *Exp. Cell Res.* **2019**, *382* (2), 111472. https://doi.org/10.1016/j.yexcr.2019.06.017.
- (50) Dykes, S. S.; Fasanya, H. O.; Siemann, D. W. Cathepsin L Secretion by Host and Neoplastic Cells Potentiates Invasion. *Oncotarget* **2019**, *10* (53), 5560–5568. https://doi.org/10.18632/oncotarget.27182.
- (51) Oelschlaegel, D.; Weiss Sadan, T.; Salpeter, S.; Krug, S.; Blum, G.; Schmitz, W.; Schulze, A.; Michl, P. Cathepsin Inhibition Modulates Metabolism and Polarization of Tumor-Associated Macrophages. *Cancers* **2020**, *12* (9), 2579. https://doi.org/10.3390/cancers12092579.
- (52) He, G.; He, M.; Wang, R.; Li, X.; Hu, H.; Wang, D.; Wang, Z.; Lu, Y.; Xu, N.; Du, J.; Fan, J.; Peng, X.; Sun, W. A Near-Infrared Light-Activated Photocage Based on a Ruthenium Complex for Cancer Phototherapy. *Angew. Chem., Int. Ed.* **2023**, *62* (24), e202218768. https://doi.org/10.1002/anie.202218768.
- (53) He, M.; Chen, F.; Shao, D.; Weis, P.; Wei, Z.; Sun, W. Photoresponsive Metallopolymer Nanoparticles for Cancer Theranostics. *Biomaterials* **2021**, *275*, 120915. https://doi.org/10.1016/j.biomaterials.2021.120915.
- Zhang, B.; Xu, Z.; Zhou, W.; Liu, Z.; Zhao, J.; Gou, S. A Light-Controlled Multi-Step Drug Release Nanosystem Targeting Tumor Hypoxia for Synergistic Cancer Therapy. *Chem. Sci.* **2021**, *12* (35), 11810–11820. https://doi.org/10.1039/D1SC01888D.
- (55) Toupin, N. P.; Steinke, S. J.; Herroon, M. K.; Podgorski, I.; Turro, C.; Kodanko, J. J. Unlocking the Potential of Ru(II) Dual-action Compounds with the Power of the Heavy-atom Effect †. *Photochem Photobiol.* **2022**, *98* (2), 378–388. https://doi.org/10.1111/php.13573.

- (56) Lameijer, L. N.; Ernst, D.; Hopkins, S. L.; Meijer, M. S.; Askes, S. H. C.; Le Dévédec, S. E.; Bonnet, S. A Red-Light-Activated Ruthenium-Caged NAMPT Inhibitor Remains Phototoxic in Hypoxic Cancer Cells. *Angew. Chem., Int. Ed.* **2017**, *56* (38), 11549–11553. https://doi.org/10.1002/anie.201703890.
- (57) Zhang, L.; Wang, P.; Zhou, X.-Q.; Bretin, L.; Zeng, X.; Husiev, Y.; Polanco, E. A.; Zhao, G.; Wijaya, L. S.; Biver, T.; Le Dévédec, S. E.; Sun, W.; Bonnet, S. Cyclic Ruthenium-Peptide Conjugates as Integrin-Targeting Phototherapeutic Prodrugs for the Treatment of Brain Tumors. *J. Am. Chem. Soc.* **2023**, *145* (27), 14963–14980. https://doi.org/10.1021/jacs.3c04855.
- (58) Karges, J.; Heinemann, F.; Maschietto, F.; Patra, M.; Blacque, O.; Ciofini, I.; Spingler, B.; Gasser, G. A Ru(II) Polypyridyl Complex Bearing Aldehyde Functions as a Versatile Synthetic Precursor for Long-Wavelength Absorbing Photodynamic Therapy Photosensitizers. *Bioorg. Med. Chem.* **2019**, *27* (12), 2666–2675. https://doi.org/10.1016/j.bmc.2019.05.011.
- (59) Ash, C.; Dubec, M.; Donne, K.; Bashford, T. Effect of Wavelength and Beam Width on Penetration in Light-Tissue Interaction Using Computational Methods. *Lasers Med. Sci.* **2017**, *32* (8), 1909–1918. https://doi.org/10.1007/s10103-017-2317-4.
- (60) Fritsch, C.; Stege, H.; Saalmann, G.; Goerz, G.; Ruzicka, T.; Krutmann, J. Green Light Is Effective and Less Painful than Red Light in Photodynamic Therapy of Facial Solar Keratoses. *Photoderm. Photoimm. Photomed.* **1997**, *13* (5–6), 181–185. https://doi.org/10.1111/j.1600-0781.1997.tb00226.x.
- (61) Sun, Y.; Joyce, L. E.; Dickson, N. M.; Turro, C. Efficient DNA Photocleavage by [Ru(Bpy)2(Dppn)]2+ with Visible Light. *Chem. Commun.* **2010**, *46* (14), 2426. https://doi.org/10.1039/b925574e.
- (62) Albani, B. A.; Peña, B.; Leed, N. A.; de Paula, N. A. B. G.; Pavani, C.; Baptista, M. S.; Dunbar, K. R.; Turro, C. Marked Improvement in Photoinduced Cell Death by a New Tris-Heteroleptic Complex with Dual Action: Singlet Oxygen Sensitization and Ligand Dissociation. *J. Am. Chem. Soc.* **2014**, *136* (49), 17095–17101. https://doi.org/10.1021/ja508272h.
- (63) Gupta, S.; Vandevord, J. M.; Loftus, L. M.; Toupin, N.; Al-Afyouni, M. H.; Rohrabaugh, T. N.; Turro, C.; Kodanko, J. J. Ru(II)-Based Acetylacetonate Complexes Induce Apoptosis Selectively in Cancer Cells. *Inorg. Chem.* **2021**, *60* (24), 18964–18974. https://doi.org/10.1021/acs.inorgchem.1c02796.
- (64) Buttle, D. J.; Murata, M.; Knight, C. G.; Barrett, A. J. CA074 Methyl Ester: A Proinhibitor for Intracellular Cathepsin B. *Arch. Biochem. Biophys.* **1992**, *299* (2), 377–380. https://doi.org/10.1016/0003-9861(92)90290-d.
- (65) Yoon, M. C.; Christy, M. P.; Phan, V. V.; Gerwick, W. H.; Hook, G.; O'Donoghue, A. J.; Hook, V. Molecular Features of CA-074 pH-Dependent Inhibition of Cathepsin B. *Biochemistry* **2022**, *61* (4), 228–238. https://doi.org/10.1021/acs.biochem.1c00684.

- (66) Montaser, M.; Lalmanach, G.; Mach, L. CA-074, but Not Its Methyl Ester CA-074Me, Is a Selective Inhibitor of Cathepsin B within Living Cells. *Biol. Chem.* **2002**, *383* (7–8), 1305–1308. https://doi.org/10.1515/BC.2002.147.
- (67) Wong, D. Y. Q.; Yeo, C. H. F.; Ang, W. H. Immuno-Chemotherapeutic Platinum(IV) Prodrugs of Cisplatin as Multimodal Anticancer Agents. *Angew. Chem., Int. Ed.* **2014**, *53* (26), 6752–6756. https://doi.org/10.1002/anie.201402879.
- (68) Ulrich, S.; Boturyn, D.; Marra, A.; Renaudet, O.; Dumy, P. Oxime Ligation: A Chemoselective Click-Type Reaction for Accessing Multifunctional Biomolecular Constructs. *Chem. Eur. J.* **2014**, *20* (1), 34–41. https://doi.org/10.1002/chem.201302426.
- (69) Collins, J.; Xiao, Z.; Müllner, M.; Connal, L. A. The Emergence of Oxime Click Chemistry and Its Utility in Polymer Science. *Polym. Chem.* **2016**, *7* (23), 3812–3826. https://doi.org/10.1039/C6PY00635C.
- (70) Hering, A.; Braga Emidio, N.; Muttenthaler, M. Expanding the Versatility and Scope of the Oxime Ligation: Rapid Bioconjugation to Disulfide-Rich Peptides. *Chem. Commun.* **2022**, *58* (65), 9100–9103. https://doi.org/10.1039/D2CC03752A.
- (71) Kölmel, D. K.; Kool, E. T. Oximes and Hydrazones in Bioconjugation: Mechanism and Catalysis. *Chem. Rev.* **2017**, *117* (15), 10358–10376. https://doi.org/10.1021/acs.chemrev.7b00090.
- (72) Dirksen, A.; Dawson, P. E. Rapid Oxime and Hydrazone Ligations with Aromatic Aldehydes for Biomolecular Labeling. *Bioconjugate Chem.* **2008**, *19* (12), 2543–2548. https://doi.org/10.1021/bc800310p.
- (73) Zhou, Q.; Lei, W.; Chen, Y.; Li, C.; Hou, Y.; Zhang, B.; Wang, X. Ruthenium(II)-Arene Complexes with Strong Fluorescence: Insight into the Underlying Mechanism. *Chem. Eur. J.* **2012**, *18* (28), 8617–8621. https://doi.org/10.1002/chem.201200960.
- (74) Tamai, M.; Matsumoto, K.; Omura, S.; Koyama, I.; Ozawa, Y.; Hanada, K. In Vitro and in Vivo Inhibition of Cysteine Proteinases by EST, a New Analog of E-64. *J. Pharmacobio-Dyn.* **1986**, *9* (8), 672–677. https://doi.org/10.1248/bpb1978.9.672.
- (75) Al-Afyouni, M. H.; Rohrabaugh, T. N.; Al-Afyouni, K. F.; Turro, C. New Ru(II) Photocages Operative with near-IR Light: New Platform for Drug Delivery in the PDT Window. *Chem. Sci.* **2018**, *9* (32), 6711–6720. https://doi.org/10.1039/C8SC02094A.
- (76) Loftus, L. M.; Al-Afyouni, K. F.; Rohrabaugh, T. N.; Gallucci, J. C.; Moore, C. E.; Rack, J. J.; Turro, C. Unexpected Role of Ru(II) Orbital and Spin Contribution on Photoinduced Ligand Exchange: New Mechanism To Access the Photodynamic Therapy Window. *J. Phys. Chem. C* **2019**, *123* (16), 10291–10299. https://doi.org/10.1021/acs.jpcc.9b01576.
- (77) Jakoš, T.; Pišlar, A.; Jewett, A.; Kos, J. Cysteine Cathepsins in Tumor-Associated Immune Cells. *Front. Immunol.* **2019**, *10*, 2037. https://doi.org/10.3389/fimmu.2019.02037.

- (78) Gondi, C. S.; Rao, J. S. Cathepsin B as a Cancer Target. *Expert Opin. Ther. Targets* **2013**, *17* (3), 281–291. https://doi.org/10.1517/14728222.2013.740461.
- (79) Sudhan, D. R.; Siemann, D. W. Cathepsin L Targeting in Cancer Treatment. *Pharmacol. Ther.* **2015**, *155*, 105–116. https://doi.org/10.1016/j.pharmthera.2015.08.007.
- (80) Karges, J.; Cohen, S. M. Rhenium(V) Complexes as Cysteine-Targeting Coordinate Covalent Warheads. *J. Med. Chem.* **2023**, *66* (4), 3088–3105. https://doi.org/10.1021/acs.jmedchem.2c02074.
- (81) Mosi, R.; Baird, I. R.; Cox, J.; Anastassov, V.; Cameron, B.; Skerlj, R. T.; Fricker, S. P. Rhenium Inhibitors of Cathepsin B (ReO(SYS)X (Where Y = S, Py; X = Cl, Br, SPhOMe-p)): Synthesis and Mechanism of Inhibition. *J. Med. Chem.* **2006**, *49* (17), 5262–5272. https://doi.org/10.1021/jm060357z.
- (82) Ofori, L. O.; Withana, N. P.; Prestwood, T. R.; Verdoes, M.; Brady, J. J.; Winslow, M. M.; Sorger, J.; Bogyo, M. Design of Protease Activated Optical Contrast Agents That Exploit a Latent Lysosomotropic Effect for Use in Fluorescence-Guided Surgery. *ACS Chem. Biol.* **2015**, *10* (9), 1977–1988. https://doi.org/10.1021/acschembio.5b00205.
- (83)Kennedy, G. T.; Holt, D. E.; Azari, F. S.; Bernstein, E.; Nadeem, B.; Chang, A.; Sullivan, N. T.; Segil, A.; Desphande, C.; Bensen, E.; Santini, J. T.; Kucharczuk, J. C.; Delikatny, E. J.; Bogyo, M.; Egan, A. J. M.; Bradley, C. W.; Eruslanov, E.; Lickliter, J. D.; Wright, G.; Singhal, S. A Cathepsin-Targeted Quenched Activity-Based Probe Facilitates Enhanced Detection of Human **Tumors** during Resection. Clin. Cancer Res. 2022, 28 3729-3741. (17),https://doi.org/10.1158/1078-0432.CCR-22-1215.
- (84) Suurs, F. V.; Qiu, S.-Q.; Yim, J. J.; Schröder, C. P.; Timmer-Bosscha, H.; Bensen, E. S.; Santini, J. T.; De Vries, E. G. E.; Bogyo, M.; Van Dam, G. M. Fluorescent Image-Guided Surgery in Breast Cancer by Intravenous Application of a Quenched Fluorescence Activity-Based Probe for Cysteine Cathepsins in a Syngeneic Mouse Model. *EJNMMI Res.* **2020**, *10* (1), 111. https://doi.org/10.1186/s13550-020-00688-0.
- (85) Karnthaler-Benbakka, C.; Koblmüller, B.; Mathuber, M.; Holste, K.; Berger, W.; Heffeter, P.; Kowol, C. R.; Keppler, B. K. Synthesis, Characterization and *in Vitro* Studies of a Cathepsin B-Cleavable Prodrug of the VEGFR Inhibitor Sunitinib. *Chem. Biodiversity* **2019**, *16* (1), e1800520. https://doi.org/10.1002/cbdv.201800520.
- (86) Van Dalen, F. J.; Verdoes, M. Inhibitory Prodrug Mechanism for Cysteine Cathepsin-Targeted Self-Controlled Drug Release. *J. Enzyme Inhibit. Med. Chem.* **2022**, *37* (1), 2566–2573. https://doi.org/10.1080/14756366.2022.2122961.
- (87) Dubowchik, G. M.; Firestone, R. A.; Padilla, L.; Willner, D.; Hofstead, S. J.; Mosure, K.; Knipe, J. O.; Lasch, S. J.; Trail, P. A. Cathepsin B-Labile Dipeptide Linkers for Lysosomal Release of Doxorubicin from Internalizing Immunoconjugates: Model Studies of Enzymatic Drug Release and Antigen-Specific In Vitro Anticancer Activity. *Bioconjugate Chem.* **2002**, *13* (4), 855–869. https://doi.org/10.1021/bc025536j.

(88) Zhang, X.; Tang, K.; Wang, H.; Liu, Y.; Bao, B.; Fang, Y.; Zhang, X.; Lu, W. Design, Synthesis, and Biological Evaluation of New Cathepsin B-Sensitive Camptothecin Nanoparticles Equipped with a Novel Multifuctional Linker. *Bioconjugate Chem.* **2016**, *27* (5), 1267–1275. https://doi.org/10.1021/acs.bioconjchem.6b00099.

Synopsis

A Ru(II)-based agent demonstrating dual action photochemotherapy and photodynamic therapy properties was conjugated to a cathepsin inhibitor, specifically designed to target the tumor microenvironment where cathepsins are overexpressed. Cathepsin inactivation results in inhibition of dysregulated proteolytic activity. Notably, this dual-action agent exhibits photoselectivity for inducing cell death in cancer cells and macrophages when activated with green light.

TOC graphic

